



Available online at [www.sciencedirect.com](http://www.sciencedirect.com)

SCIENCE @ DIRECT®

Journal of Hydrology 294 (2004) 68–86

Journal  
of  
Hydrology

[www.elsevier.com/locate/jhydrol](http://www.elsevier.com/locate/jhydrol)

# Transport in heterogeneous sediments with multimodal conductivity and hierarchical organization across scales

Zhenxue Dai<sup>a,\*</sup>, Robert W. Ritzi Jr.<sup>a</sup>, Chaocheng Huang<sup>b</sup>,  
Yoram N. Rubin<sup>c</sup>, David F. Dominic<sup>a</sup>

<sup>a</sup>Department of Geological Sciences, Wright State University, Dayton, OH 45435, USA

<sup>b</sup>Department of Mathematics and Statistics, Wright State University, Dayton, OH 45435, USA

<sup>c</sup>Department of Civil and Environmental Engineering, University of California, 435 Davis Hall, Berkeley, CA 94720-1710, USA

Received 6 May 2003; revised 24 July 2003; accepted 20 October 2003

## Abstract

We consider here the Lagrangian approach for stochastic modeling of the transport of inert solutes in porous media. A general global covariance function of log conductivity in sediments with hierarchical organization has been developed by combining proportions, transition probabilities, and covariances of log conductivity. The global integral scale is derived from the global covariance function with two types of correlation lengths: integral scales of local log conductivity and correlation scale of indicator space functions. The macrodispersion coefficients have been derived for the solute transport in two- and three-dimensional domains. An example is used to illustrate the time evolution trends and the relative contributions of the auto and cross terms. Sensitivity analysis indicates that the values of macrodispersion coefficients are positively related to the changes of indicator correlation scale, integral scale and the difference of the mean log conductivity between different units. But, in this example the macrodispersion coefficients are more sensitive to the indicator correlation scale than to the integral scale. The cross term in the macrodispersion coefficients has an increasing contribution when the contrast of the mean log conductivity increases. Under the condition of high contrast of log conductivity between different units, only the cross terms contribute to the macrodispersion coefficients and the auto terms can be ignored. At the large time limit, the longitudinal coefficient shows clearly a linear dependence on the global variance of log conductivity.

© 2004 Elsevier B.V. All rights reserved.

**Keywords:** Transition probability; Sedimentary units; Global covariance; Hierarchical organization; Stochastic; Microdispersion

## 1. Introduction

The Lagrangian approach was introduced in stochastic modeling of solute transport in porous media by Dagan (1982) and has received significant attention since, as reviewed by Gelhar (1993), Neuman (1997), Rubin (1997), Rubin et al. (1999) and Zhang (2002). Early work with the Lagrangian

\* Corresponding author. Tel.: +1-937-775-2478.

E-mail addresses: [zhenxue.dai@wright.edu](mailto:zhenxue.dai@wright.edu) (Z. Dai); [rritzi@wright.edu](mailto:rritzi@wright.edu) (R.W. Ritzi Jr.); [chuang@gauss.math.wright.edu](mailto:chuang@gauss.math.wright.edu) (C. Huang); [rubin@ce.berkeley.edu](mailto:rubin@ce.berkeley.edu) (Y.N. Rubin); [ddominic@wright.edu](mailto:ddominic@wright.edu) (D.F. Dominic).

approach assumed that log conductivity could be represented by a single, finite integral scale representing the spatial correlation of log conductivity. Recently, attention has been focused on representing log conductivity across different scales so that the integral scale may be neither finite nor single valued. Some work has sought to characterize the scaling of the variance and correlation of log conductivity, or alternatively the macrodispersivity, through considering a multitude of field observations and scaling experiments, and has posed a general scaling model (Neuman, 1990, 1997; Glimm et al., 1993). Some work has used these and other models for the scaling of spatial correlation of log conductivity and illustrated the resulting behavior of solute spreading (Dagan, 1994; Cushman et al., 1994; Di Federico and Neuman, 1998). In most of the prior work there has not been a strong link between the model for the spatial correlation of log conductivity and the geology it is supposed to represent.

In this paper the Lagrangian approach will be used to derive the global covariance functions and the macrodispersion coefficients for conservative solute transport through a heterogeneous formation with hierarchical organization. This approach is attractive because it offers the possibility of relating preasymptotic behavior of the macrodispersion coefficients to the sedimentary architecture. We first consider the geology, specifically that of unconsolidated sediment resulting from fluvial deposition, the source of much ground-water abstraction. We discuss how the univariate and spatial bivariate statistics for log-conductivity at different scales are related to the organization of the sediment across a range of scales. We then study how this organization affects macrodispersivity.

Importantly, Dagan (1994) has shown that the heterogeneity that affects dispersion is that which is characterized by scales smaller than the scale of the plume. Therefore, our perspective is that of a plume spreading within the limits of a fluvial deposit, and we focus on the scales of heterogeneity sampled by the plume within such a deposit. In this light, our work is related to that of Rubin (1995) which considers a finite geologic domain made of mutually exclusive regions, and is a direct extension of that work. We do not attempt to address scaling issues in a universal way nor do we address evolving scales of heterogeneity,

and thus this work is only indirectly related to work on universal scaling models cited in the paragraph above. Furthermore, the analysis here is limited to a range of scales over which log conductivity is weakly multimodal. This is true when there are slight but statistically significant differences in the univariate statistics on log conductivity among the populations taken within each sedimentary unit (e.g. as measured by Titzel (1997) and Ritzi et al. (2002)). The modes of log conductivity change at each hierarchical level in the organization of the sediment.

The Lagrangian approach requires a model for the univariate and spatial bivariate moments for log conductivity. Recent work presented such models for bimodal domains (Rubin, 1995), multimodal domains (Elfeki et al., 1997, 2002; Lu and Zhang, 2002; Barrash and Clemo, 2002; Zhang and Lu, 2002), and hierarchical multimodal domains (Ritzi et al., 2002, 2004 and Dai et al., 2004). Here we use the hierarchical multimodal models for developing the Lagrangian transport model.

Section 2 summarizes the relevant aspects of sedimentary architecture. Section 3 describes the corresponding identities for the univariate and spatial bivariate statistics on log conductivity. In Section 4, we present some derivations of a Lagrangian solute transport model with those log-conductivity identities. The goal is to show what is currently mathematically tractable and what remains as a future challenge. Furthermore, for the transport models that are tractable, we study how the pre- and postasymptotic macrodispersivities are related to characteristics of the sedimentological architecture and the resulting scales of heterogeneity in a synthetic example. Finally, we show that the derived macrodispersion coefficients in two- (2D) and three-dimensional (3D) domains can be simplified for some cross-bedded deposits with significant conductivity differences among different units, and that the macrodispersion is predominantly determined by the correlation across and the variability of geometry within different units.

## 2. Sedimentary architecture

Sedimentologists often describe sedimentary deposits using a hierarchical framework. Such a framework was related to hydrogeologically relevant

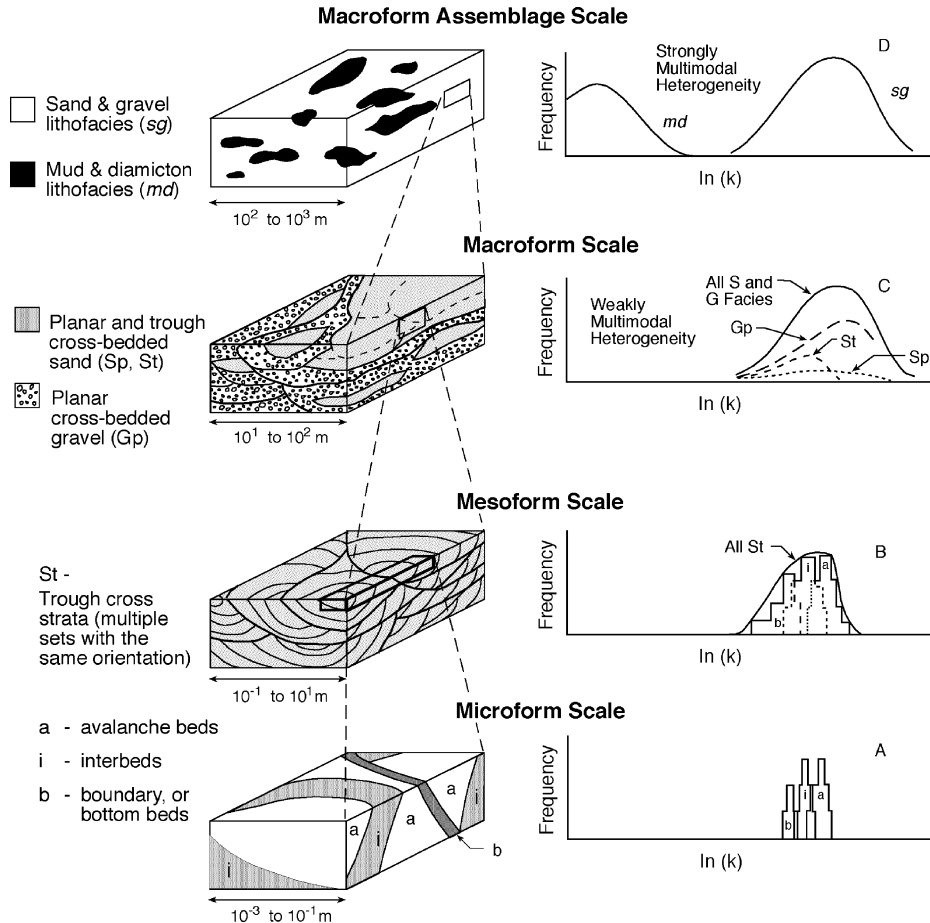


Fig. 1. Conceptual framework of the unconsolidated glacio-fluvial sediments with hierarchical organization (adapted from Ritzi et al., 2002). (A) Microform scale, (B) mesoform scale—variance increases in modes for microforms relative to (A) as larger volume is sampled, (C) macroform scale. Abscissa is rescaled from (B). (D) Macroform scale.

scales by Scheibe and Freyberg (1995), is briefly reviewed here, and is shown in Fig. 1. In the figure we portray sedimentary units defined at each level in a four-tiered hierarchy together with log conductivity populations within units at each level. Note that this hierarchy represents one organizational framework and that others are possible. However, the models developed below are not limited to the particular organization utilized here.

**Microforms.** Fig. 1A represents the lowest level in the hierarchy and will be referred to as the microform scale. Here the sediment is organized into laminae (<1 cm thick) or beds (>1 cm thick). The ones represented here are formed by the migration of bedforms such as subaqueous dunes and ripples.

For a recent review of deposition associated with fluvial bedforms see Bridge (2003). Importantly, sediment is partly sorted by size during deposition. Among the possible bed types are avalanche beds, interbeds, and bounding beds (Scheibe and Freyberg, 1995). Avalanche beds are formed by intermittent avalanches down the lee side of advancing dunes or ripples. Interbeds are formed during a relative increase in deposition of suspended sediment on the lee side of dunes or ripples caused by decreases in flow velocity due to turbulence or minor changes in bed geometry. Interbeds have a smaller average grain size than avalanche beds. Bounding beds are formed by deposition in the trough region downstream of advancing dunes or ripples. They have a large

proportion of grains deposited from suspension and generally have an average grain size smaller than either avalanche beds or interbeds. The contrast in grain size across the contacts between beds is one reason we can discern bedding.

As a single bedform passes, a group of avalanche bed, interbed, and bounding bed microforms is deposited. The histograms in Fig. 1a are meant to represent the log conductivity mode of each microform type within a single group of microforms. Ritzi et al. (2004) showed that the global log-conductivity semivariogram among sets of units approaches an exponential structure as the coefficient of variation in the lengths of the units increases toward unity.

Note that the Lagrangian approach to solute transport modeling adopted below depends upon Darcy's law and defining conductivity at scales larger than pores. Each microform is many times thicker than individual pores and microforms are, in fact, the smallest units that would be appropriate to define in this context.

*Mesoforms.* Fig. 1B shows the next higher hierarchical level. At this level, microforms are organized into mesoforms, which are units with characteristic groupings of one or more microform types. Mesoforms are bounded by surfaces across which there are distinct changes in microform types or their proportion, orientation, or average grain size. Mesoforms represent depositional episodes longer in duration than those which create microforms. In fluvial systems, a single bank-full flood might deposit a series of mesoforms. Subsequent floods might deposit similar (or different) mesoforms. Depicted in Fig. 1B is a portion of a mesoform composed of multiple sets of trough-shaped cross-strata. Each set contains alternating avalanche beds and interbeds. If boundary beds are present, they will occur between sets. Such trough cross-sets are created under specific conditions of flow depth, flow velocity and grain size and are oriented with avalanche beds and interbeds dipping parallel to the prevailing direction of flow during deposition. Thus, the trough cross-sets within a single mesoform will have a common orientation.

Although not depicted in Fig. 1, mud drapes are another mesoform type (see Scheibe and Freyberg, 1995). When flow depth and velocity diminish during the waning stage of a flood, fine sediment deposited from suspension drapes the previous sediment

surface. Such layers may be variable in thickness but normally are uniformly fine grained with low permeability. Because of this uniformity, this mesoform is composed of a single microform type.

At the mesoform scale we might have the same modes as at microform scale, with the variance in each log conductivity mode larger than that measured in a single set (Fig. 1A), reflecting more diversity in deposition over the time in which many more microform sets were deposited.

*Macroforms.* Mesoforms are organized into macroforms (Fig. 1C). The figure shows multiple mesoforms including the trough cross-bedded mesoform of Fig. 1B, along with planar cross-bedded sand and planar cross-bedded gravel mesoforms, as might occur in a channel belt. The macroform is a larger feature representing the cumulative effect of multiple depositional events over a long period of time. Here the difference in log conductivity modes between mesoforms is depicted to be greater than the difference in modes between microforms defined at the mesoform scale. There may be significant overlap in the modes, creating weakly multimodal heterogeneity at this level.

*Macroform assemblage.* Fig. 1D represents a fourth hierarchical level of organization, a macroform assemblage scale, in which two macroform types occur. The macroforms are shown to have a strongly bimodal log conductivity distribution, as quantified in glacio-fluvial channel belt sediments by Ritzi et al. (2002). The macroform assemblage as depicted in the figure is intended to convey the level at and beyond which the solute transport models developed below would not be appropriate. One issue is that when the global variance in log conductivity exceeds unity an assumption in the derivations is violated. However, Lagrangian macrodispersivity models have been shown to be fairly robust to that assumption, as shown, for example, by Rubin (1995) in an application to strongly bi-modal log conductivity arising in sand-shale sequences (see also discussion by Desbarats (1990) and Rubin (1997)). More importantly, the lumped measure of solute spreading that the macrodispersivity represents is no longer of interest to us when transport behavior shows large differences between faster transport in preferential flow pathways, and long residence time in low-conductivity regions (Ritzi et al., 2000). Thus, we

limit the analysis to plumes that exist over scales captured in the first three hierarchical levels, which would include the overall scale of some of the better known natural-gradient tracer tests, e.g. Borden (Sudicky, 1986) and Cape Cod (Leblanc et al., 1991).

### 3. Univariate and spatial bivariate statistics on log conductivity

Rubin (1995) derived expressions for the mean, variance and spatial covariance of log conductivity for the bimodal case. The log conductivity is modeled with a continuous space function and the presence of units is modeled with an indicator space function. In this work and that by Rubin and Journel (1991) and Russo et al. (2001) the correlation structures of the indicator variables were assigned somewhat arbitrarily, without specifying how the mean, variance, and shape and range of the indicator correlation function are related to the proportions, geometry, and pattern of the sedimentary units they represent.

The expressions were expanded by Lu and Zhang (2002) to include any number of modes. Importantly, Lu and Zhang (2002) incorporated the work of Carle and Fogg (1996, 1997) which relates the structure of the indicator random variables to proportions, geometry and pattern of the units. For bimodal media, they explored the sensitivity of the global variance of  $Y(x)$  to the proportions of the units, the difference in mean conductivity across the units, and the variance in conductivity within each unit. The integral scales for the spatial correlation of conductivity within units were shown to be limited by the indicator integral scales: the effective range of the log conductivity correlation should not be expected to exceed the mean length of the units. They concluded that the integral scale of the composite log conductivity field may be larger or smaller than that of the indicator function. Barrash and Clemo (2002) gave a multimodal model, weighting local semivariograms of units with empirical coefficients for a specific deposit, in developing an understanding of the relationship of global and local semivariograms.

Ritzi et al. (2004) and Rubin (2003) presented a general form of a hierarchical, multimodal correlation model. This general model can be simplified to the forms of the other models referenced above.

While the model can be written with any number of hierarchical levels, here we write it in the form of a macroform (global scale) made up of mesoforms, and mesoforms made up of microforms.

#### 3.1. Relevant geostatistical identities

Consider a domain made up of  $N$  mesoforms filling space in mutually exclusive occurrences. The mesoform regions are made up of  $N_o$  (or  $N_j$ ,  $o, j = \overline{1, N}$ ) types of microforms, also occurring as mutually exclusive entities. Take two points,  $\mathbf{x}$  and  $\mathbf{x}'$ , separated by a vector  $\mathbf{h}$  with magnitude  $h$ .  $\mathbf{x}$  occurs in microform  $k$  which is in mesoform  $o$  and  $\mathbf{x}'$  within microform  $i$  which is in mesoform  $j$ . Log conductivity at location  $x$  is given by  $Y_{ok}(\mathbf{x})$ . The indicator space function  $I_{ok}(\mathbf{x})$  is defined:

$$I_{ok}(\mathbf{x}) = \begin{cases} 1, & \text{if microform } k \text{ occurs in mesoform } o \\ & \text{at location } \mathbf{x} \\ 0, & \text{otherwise.} \end{cases} \quad (1)$$

The global log conductivity  $Y_{ok}(\mathbf{x})$  can be expressed as

$$Y(\mathbf{x}) = \sum_{o=1}^N \sum_{k=1}^{N_o} I_{ok}(\mathbf{x}) Y_{ok}(\mathbf{x}). \quad (2)$$

If the volume proportion of region  $ok$  is  $p_{ok}$ , then  $\sum_{o=1}^N \sum_{k=1}^{N_o} p_{ok} = 1$ , and the expected value of  $I_{ok}$  is equal to  $p_{ok}$ . The global mean  $M_Y$  and variance  $\sigma_Y^2$  of log conductivity can be derived as

$$M_Y = \sum_{o=1}^N \sum_{k=1}^{N_o} p_{ok} m_{ok}, \quad (3)$$

$$\sigma_Y^2 = \sum_{o=1}^N \sum_{k=1}^{N_o} p_{ok} \sigma_{ok}^2 + \frac{1}{2} \sum_{o=1}^N \sum_{j=1}^N \sum_{k=1}^{N_o} \sum_{i=1}^{N_j} p_{ok} p_{ji} (m_{ok} - m_{ji})^2, \quad (4)$$

where  $m_{ok}$  and  $\sigma_{ok}^2$  denote the mean and variance of  $Y_{ok}(\mathbf{x})$ , respectively (Ritzi et al., 2004).

As applied to measuring spatial continuity, the transition probability denotes the conditional probability (Carle and Fogg, 1996; Ritzi, 2000). By using indicator variables, the transition probability  $t_{ok,ji}(\mathbf{h})$

for the sedimentary units is given by

$$t_{ok,ji}(\mathbf{h}) = \Pr\{I_{ji}(\mathbf{x}') = 1 \text{ and } I_{ok}(\mathbf{x}) = 1\} / \Pr\{I_{ok}(\mathbf{x}) = 1\}. \quad (5)$$

The global semivariogram of log conductivity,  $\gamma_Y(\mathbf{h})$ , can be expressed as a function of the proportions, the transition probabilities and the in-facies or cross-facies correlation of  $Y_{ok}(\mathbf{x})$  as

$$\gamma_Y(\mathbf{h}) = \sum_{o=1}^N \sum_{j=1}^N \sum_{k=1}^{N_o} \sum_{i=1}^{N_j} \gamma_{ok,ji}(\mathbf{h}) p_{ok} t_{ok,ji}(\mathbf{h}), \quad (6)$$

where  $\gamma_{ok,ji}(\mathbf{h})$  is the semivariogram within ( $o, k = j, i$ ) or cross-facies ( $o, k \neq j, i$ ) (Ritzi et al., 2004).

Similarly, the global centered covariance  $C_Y(\mathbf{h})$  can be written as

$$C_Y(\mathbf{h}) = \sum_{o=1}^N \sum_{j=1}^N \sum_{k=1}^{N_o} \sum_{i=1}^{N_j} \{C_{ok,ji}(\mathbf{h}) + m_{ok} m_{ji}\} \\ \times p_{ok} t_{ok,ji}(\mathbf{h}) - M_Y^2, \quad (7)$$

where  $C_{ok,ji}(\mathbf{h})$  is the covariance of  $[Y_{ok}(\mathbf{x}), Y_{ji}(\mathbf{x}')]$ .

Eq. (7) is an exact identity in relating the global covariance to the univariate and bivariate statistics for units defined at the lower hierarchical levels. With  $N = 1$ , the covariance Eq. (7) matches that of Lu and Zhang (2002) and if  $N_o = 2$ , Eqs. (4) and (7) become the same as those derived by Rubin (1995) for the bimodal model. Ritzi et al. (2004) showed the exact equivalency of the right and left hand sides using sample statistics computed from exhaustively sampled data representing cross-bedded sediments in a point-bar deposit. That was a deterministic study that showed that the hierarchical and multimodal covariance model is relevant in representing real and complex geologic architecture.

### 3.2. Required assumptions and relation to geologic architecture

To use the identity in the Lagrangian framework the only conceptual assumption that we must make is that the statistical attributes are stationary (weak sense for the bivariate statistics), as in the probabilistic form used in writing Eq. (7).

However, there are a number of other assumptions that we must make in order to make derivations of

macrodispersion models tractable if using the hierarchical model. First of all, we must assume a functional form for both  $C_{ok,ji}(\mathbf{h})$  and  $t_{ok,ji}(\mathbf{h})$ . An exponential model is commonly assumed for each (Lu and Zhang, 2002; Dai et al., 2004), and is in fact required to make the derivations presented below tractable. Ritzi et al. (2004) addressed this question, studying the hierarchical architecture of cross-bedded sedimentary deposits. It was shown that in such deposits, units at higher hierarchical levels are typically made up of repeated occurrences of units defined at the next lower level.

Importantly, there is a difference in mean grain size, and consequently in  $Y(\mathbf{x})$ , across the boundaries of these units, as illustrated among the modes defined at different scales in Fig. 1. Thus, most of the variance arises from differences across units rather than within units. It is shown by Ritzi et al. (2004) that under these conditions, the shape of  $C_Y(\mathbf{h})$  is defined by that of the transition probabilities. Ritzi (2000) and Ritzi et al. (2004) showed that the transition probabilities in this type of architecture will be exponential if the units are sampled in relatively large numbers and the variance in the length among the units sampled is large (i.e. the coefficient of variation approaches unity). Thus, the exponential model we assume here represents a deposit with repeated units having variation in the length of the units. Examples of such architecture are easy to find, such as at the well-studied Borden and Cape Cod sites. Ritzi et al. (2004) showed that the coefficient of variation in lengths when sampled in different directions (e.g. parallel to the strike, parallel to the dip, or normal to the bedding of units) may be anisotropic. In particular, the variance was lowest in the vertical and highest along strike. When the coefficient of variation is smaller, the transition probabilities rise as does a linear or spherical function and have periodicity beyond the sill. We cannot represent such complicated structures in the derivations below but must assume an exponential shape in all directions. In doing so, we may be over-representing the variability in the length of the units. While we can say that the derivations using exponential models represent a common type of sedimentary deposit, we cannot say what other types of geologic scenarios, if any, it represents.

We also assume that the cross-covariances are negligible, i.e.  $C_{ok,ji}(\mathbf{h}) = 0, \forall ok \neq ji$ . This is

a common assumption (e.g. Rubin, 1995) and it is supported in results by Dai et al. (2004) and Ritzi et al. (2004). In assuming this, we can write Eq. (7) in the following form (see Appendix A):

$$C_Y(\mathbf{h}) = \sum_{o=1}^N \sum_{k=1}^{N_o} p_{ok} C_{ok,ok}(\mathbf{h}) t_{ok,ok}(\mathbf{h}) + \frac{1}{2} \sum_{o=1}^N \sum_{j=1}^N \sum_{k=1}^{N_o} \sum_{i=1}^{N_j} (m_{ok} - m_{ji})^2 \times p_{ok}(p_{ji} - t_{ok,ji}(\mathbf{h})). \quad (8)$$

Another assumption we must make is that the auto-covariances and transition probabilities have an isotropic correlation scale along strike and dip directions of the mean flow vector. We can allow for anisotropy in the vertical direction. Appendix B shows the proof that all auto- and cross-transition probabilities of the units within the same hierarchical level have a uniform indicator correlation scale. Therefore, the transition probabilities and auto-covariances in a 3D domain can be expressed by exponential functions with principal spatial correlation scales,  $\lambda_I$ ,  $\lambda_{ok}$  and  $\lambda_{zI}$ ,  $\lambda_{zok}$  corresponding to Cartesian coordinate directions  $x$  or  $y$ , and  $z$ , respectively

$$t_{ok,ji}(\mathbf{h}_I) = p_{ji} + (\delta_{ok,ji} - p_{ji})e^{(-h_I/\lambda_I)} \quad (9)$$

for  $o, j = \overline{1, N}$ ;  $k = \overline{1, N_o}$ ;  $i = \overline{1, N_j}$ ,

$$C_{ok,ok}(\mathbf{h}_{ok}) = \sigma_{ok}^2 e^{(-h_{ok}/\lambda_{ok})} \quad (10)$$

for  $o = \overline{1, N}$ ;  $k = \overline{1, N_o}$ ,

$$\mathbf{h}_{ok} = \sqrt{x^2 + y^2 + \varepsilon_{ok}^{-2} z^2}, \quad \varepsilon_{ok} = \lambda_{zok}/\lambda_{ok}.$$

Furthermore, to make the derivation of macro-dispersion coefficients tractable under the methods that are known, we must assume that the anisotropy is the same for both the indicator and permeability correlation. Thus,  $\varepsilon_{ok} = \varepsilon_I = \varepsilon$ , we have

$$\tilde{h} = \mathbf{h}_{ok} = \mathbf{h}_I = \sqrt{x^2 + y^2 + \varepsilon^{-2} z^2}. \quad (11)$$

Substituting Eqs. (9) and (10) into Eq. (8), we obtain the vertically anisotropic covariance function

$$C_Y(\tilde{h}) = \sum_{o=1}^N \sum_{k=1}^{N_o} p_{ok}^2 \sigma_{ok}^2 e^{(-\tilde{h}/\lambda_{ok})} + \sum_{o=1}^N \sum_{k=1}^{N_o} p_{ok}(1 - p_{ok}) \sigma_{ok}^2 e^{(-\tilde{h}/(\lambda_{ok}\lambda_I/(\lambda_{ok} + \lambda_I)))} + \frac{1}{2} \sum_{o=1}^N \sum_{j=1}^N \sum_{k=1}^{N_o} \sum_{i=1}^{N_j} (m_{ok} - m_{ji})^2 p_{ok} p_{ji} e^{(-\tilde{h}/\lambda_I)} \quad (12)$$

### 3.3. Global integral scale

According to Dagan (1989), the global integral scale  $\lambda_Y$  is defined as:

$$\lambda_Y = \frac{1}{\sigma_Y^2} \int_0^\infty C_Y(\tilde{h}) d\tilde{h}. \quad (13)$$

Then, by using Eq. (12) we obtain the formulation of global integral scale as

$$\lambda_Y = \frac{\sum_{o=1}^N \sum_{k=1}^{N_o} p_{ok}^2 \sigma_{ok}^2 \lambda_{ok} + \sum_{o=1}^N \sum_{k=1}^{N_o} p_{ok}(1 - p_{ok}) \sigma_{ok}^2 \frac{\lambda_{ok}\lambda_I}{\lambda_{ok} + \lambda_I} + \frac{1}{2} \sum_{o=1}^N \sum_{j=1}^N \sum_{k=1}^{N_o} \sum_{i=1}^{N_j} p_{ok} p_{ji} (m_{ok} - m_{ji})^2 \lambda_I}{\sum_{o=1}^N \sum_{k=1}^{N_o} p_{ok} \sigma_{ok}^2 + \frac{1}{2} \sum_{o=1}^N \sum_{j=1}^N \sum_{k=1}^{N_o} \sum_{i=1}^{N_j} p_{ok} p_{ji} (m_{ok} - m_{ji})^2} \quad (14)$$

where  $\delta_{ok,ji}$  is the Kronecker delta

$$\mathbf{h}_I = \sqrt{x^2 + y^2 + \varepsilon_I^{-2} z^2}, \quad \varepsilon_I = \lambda_{zI}/\lambda_I,$$

From Eq. (14), one can see that the global integral scale depends on proportions, variances and integral scales of  $Y_{ok}(\mathbf{x})$ , and indicator correlation scale. Its value will increase with the increase in  $\lambda_{ok}$  and  $\lambda_I$ .

Table 1  
Coefficients for  $\alpha_{mok}$  and  $\eta_{mok}$  (for  $o, j = \overline{1, N}, k = \overline{1, N_o}, i = \overline{1, N_j}$ )

$m$	1	2	3
$\alpha_{mok}$	$\lambda_{ok}$	$\frac{\lambda_{ok}\lambda_I}{\lambda_{ok} + \lambda_I}$	$\lambda_I$
$\eta_{mok}$	$\sigma_{ok}^2 p_{ok}^2$	$\sigma_{ok}^2 p_{ok}(1 - p_{ok})$	$\frac{1}{2} \sum_{j=1}^N \sum_{i=1}^{N_j} p_{ok} p_{ji} (m_{ok} - m_{ji})^2$

If we define  $\Delta\lambda = \lambda_Y - \lambda_I$ , then

$$\Delta\lambda = \frac{1}{\sigma_Y^2} \sum_{o=1}^N \sum_{k=1}^{N_o} p_{ok} \sigma_{ok}^2 \frac{p_{ok}\lambda_{ok}^2 - \lambda_I^2}{\lambda_{ok} + \lambda_I}.$$

If  $\lambda_{ok} \leq \lambda_I$ , and  $p_{ok} < 1$ , then  $p_{ok}\lambda_{ok}^2 - \lambda_I^2 < 0$  (for  $o = \overline{1, N}; k = \overline{1, N_o}$ ). The condition  $\lambda_{ok} \leq \lambda_I$  is true for most cases, such as the examples in Lu and Zhang (2002, Table 1) and Dai et al. (2004). In this case,  $\lambda_Y < \lambda_I$ . That is, the global integral scale of the log conductivity is smaller than indicator correlation scale,  $\lambda_I$ . However, in the case that  $\lambda_{ok} \geq \lambda_I/\sqrt{p_{ok}}$ ,  $\lambda_Y \geq \lambda_I$ .

Furthermore, in the case that  $\sigma_{ok}^2 \rightarrow 0$  (for  $o = \overline{1, N}; k = \overline{1, N_o}$ ) or when the contrast in the mean log conductivity between any two units is relatively large, the global integral scale is close to the indicator correlation scale  $\lambda_I$ , or

$$\lambda_Y \approx \lambda_I. \tag{15}$$

Therefore, we conclude that the global integral scale might be smaller, equal to, or larger than the indicator correlation scale, but usually will be smaller. The impact of the high contrast in log conductivity to macrodispersion will be discussed in Section 5.

#### 4. Derivation of macrodispersion coefficients

In order to evaluate a macroscopic dispersivity tensor  $D_{pq}(t)$ , it is necessary to relate the spectrum of the local flow variation to that of the local log conductivity perturbations. This relationship depends on the covariance of log conductivity in the multimodal hierarchical media. Our derivations of the macrodispersion coefficients follow from the equation

of Dagan (1988, 1989) and Rubin (1995, 2003)

$$\widehat{u}_{pq}(\mathbf{k}) = U_1^2 \left( \delta_{1p} - \frac{k_p k_1}{k^2} \right) \left( \delta_{1q} - \frac{k_q k_1}{k^2} \right) \widehat{C}_Y(\mathbf{k}) \tag{16}$$

$(p, q = 1, \dots, d)$

where  $u_{pq}$  is the velocity covariance in real space, the circumflex denotes the Fourier transform operator,  $U_1 = \exp(M_Y)\mathbf{g}_1/n$  is the mean velocity assuming that the  $x$  direction is aligned with the mean velocity direction,  $\mathbf{g}_1$  is the mean hydraulic gradient in that direction,  $\delta_{1p}$  is the Kronecker delta,  $k$  is the modulus of the vector  $\mathbf{k}$ , and  $d$  denotes space dimensionality.

In deriving Eq. (16), Rubin (1995, 2003) made the following assumptions: (1) the flow field is at steady state, (2) the conductivity field is weakly stationary, (3) the velocity field is uniform in the mean, (4) the flow domain is unbounded, and (5) variance of the log conductivity  $\sigma_Y^2$  is smaller than unity. Furthermore, assuming that the mean displacement velocity of a solute particle is approximated at first order by the average fluid velocity of a solute particle is approximated at first order by the average fluid velocity, the macrodispersion coefficients are computed by

$$D_{pq}(t) = \int_0^t u_{pq}(U_1 t') dt' \tag{17}$$

By using Eqs. (12), (16) and (17), we can derive the macrodispersion coefficients for different directions and dimensions.

##### 4.1. Three-dimensional results

Dagan (1989) derived the 3D macrodispersivity with a unimodal covariance (a single exponential function). Following the steps described by Dagan (1989, p. 314–315), we develop the longitudinal, lateral and transverse macrodispersion coefficients for the sediments with hierarchical-multimodal permeability

$$\begin{aligned} \frac{D_{11}(t)}{U_1} = & \sum_{m=1}^3 \sum_{o=1}^N \sum_{k=1}^{N_o} \alpha_{mok} \eta_{mok} \left\{ 1 - e^{(-\tau_{mk})} \right. \\ & - \varepsilon \int_0^\infty \left( 2R\mathbf{J}_1(\beta) \frac{2u^{3/2} - \varepsilon R(2u + v)}{v^2 u^{3/2}} \right. \\ & \left. \left. + F(R) \right) dR \right\}, \end{aligned}$$

$$F(R) = \frac{(2 - \beta^2)\mathbf{J}_1(\beta) - \beta\mathbf{J}_0(\beta)}{R\tau_{mok}^2} \times \left( \frac{\varepsilon^3 R^3(4u + v) + (5v - 4u)u^{3/2}}{v^3 u^{3/2}} \right), \quad (18)$$

$$\frac{D_{22}(t)}{U_1} = \sum_{m=1}^3 \sum_{o=1}^N \sum_{k=1}^{N_o} \alpha_{mok} \eta_{mok} \varepsilon \int_0^\infty \frac{2\mathbf{J}_1(\beta) - \beta\mathbf{J}_0(\beta)}{\tau_{mok}^2} \times \left( \frac{\varepsilon^3 R^3(4u + v) + (5v - 4u)u^{3/2}}{Rv^3 u^{3/2}} \right) dR, \quad (19)$$

$$\frac{D_{33}(t)}{U_1} = \sum_{m=1}^3 \sum_{o=1}^N \sum_{k=1}^{N_o} \alpha_{mok} \eta_{mok} \varepsilon \int_0^\infty R\mathbf{J}_1(\beta) \times \left( \frac{u^{1/2}(4u - 3v) - \varepsilon R(4u - v)}{v^3 u^{1/2}} \right) dR, \quad (20)$$

where  $\beta = R\tau_{mok}$ ,  $u = 1 + R^2$ ,  $v = 1 + R^2 - \varepsilon^2 R^2$ ,  $\tau_{mok} = tU_1/\alpha_{mok}$ . The coefficients  $\alpha_{mok}$  and  $\eta_{mok}$  can be found in Table 1.  $\mathbf{J}_0$  and  $\mathbf{J}_1$  are the zero and first order Bessel functions, respectively.  $R$  is the variable of integration.

The expressions in Eqs. (18), (19) and (20) cannot be integrated in closed form. We use numerical integration to evaluate them at a number of points in the parameter space, and present the results in Section 5.

In the case of 3D isotropy,  $\varepsilon = 1$ , and the integrations (18) and (19) can be carried out to obtain closed-form 3D analytical solutions

$$\frac{D_{11}(t)}{U_1} = \sum_{m=1}^3 \sum_{o=1}^N \sum_{k=1}^{N_o} \alpha_{mok} \eta_{mok} \left\{ 1 + \frac{4}{e^{\tau_{mok}} \tau_{mok}^4} \times [6(e^{\tau_{mok}} - \tau_{mok} - 1) - \tau_{mok}^2(e^{\tau_{mok}} + 2)] \right\} \quad (21)$$

$$\frac{D_{22}(t)}{U_1} = \frac{D_{33}(t)}{U_1} = \sum_{m=1}^3 \sum_{o=1}^N \sum_{k=1}^{N_o} \alpha_{mok} \eta_{mok} \left\{ \frac{1}{e^{\tau_{mok}} \tau_{mok}^4} \times [12(1 + \tau_{mok} - e^{\tau_{mok}}) + \tau_{mok}^2(5 + e^{\tau_{mok}} + \tau_{mok})] \right\} \quad (22)$$

#### 4.2. Two-dimensional results

In particular, for a 2D isotropic velocity field, the macrodispersion coefficients (18) and (19) can be simplified to 2D results. The longitudinal and transverse macrodispersion coefficients are given by

$$\frac{D_{11}(t)}{U_1} = \sum_{m=1}^3 \sum_{o=1}^N \sum_{k=1}^{N_o} \alpha_{mok} \eta_{mok} \left\{ 1 + \frac{3}{2e^{\tau_{mok}} \tau_{mok}^3} \times [2(e^{\tau_{mok}} - \tau_{mok} - 1) - e^{\tau_{mok}} \tau_{mok}^2] \right\} \quad (23)$$

$$\frac{D_{22}(t)}{U_1} = \sum_{m=1}^3 \sum_{o=1}^N \sum_{k=1}^{N_o} \alpha_{mok} \eta_{mok} \times \left\{ \frac{6(1 - e^{\tau_{mok}} + \tau_{mok}) + 2\tau_{mok}^2 + e^{\tau_{mok}} \tau_{mok}^2}{2e^{\tau_{mok}} \tau_{mok}^3} \right\} \quad (24)$$

Note that when  $N = 1$  and  $N_o = 2$ , Eqs. (23) and (24) are equivalent to the expressions obtained by Rubin (1995) for bimodal log conductivity.

When comparing Eqs. (18)–(24) with the global covariance Eqs. (8) and (12), we can see that the sum of the  $m = 1, 2$  terms in these equations corresponds to the first term in Eq. (8), which is made of the auto-covariances of  $Y_{ok}(\mathbf{x})$  as weighted by the proportion and auto-transition probabilities. So, this sum is called the auto term. The  $m = 3$  term in Eqs. (18)–(24) corresponds to the second term in Eq. (8), which represents the expected difference in  $Y_{ok}(\mathbf{x})$  (or the contrast in the mean) across the unit boundaries as weighted by the cross-transition probabilities. So, it

Table 2  
The parameters used for computing the macrodispersion coefficients

Mesoform (o)	Microform (k)	$\rho_{ok}$	$K_{Gok}$ (m/d)	$m_{ok}$	$\lambda_{ok}$ (m)	$\sigma_{ok}^2$	$\lambda_l$ (m)
1	1	0.2	0.1	-2.303	3	0.1	10
2	1	0.5	0.5	-0.693	5	0.2	10
	2	0.3	1.0	0	3	0.3	10

is called the cross term. The relative contributions of these terms to the macrodispersion coefficients will be discussed in Section 5.

### 5. Discussion of results

Table 2 gives a set of parameters that define a formation with three hierarchical levels. The global domain is made of two mesoform types which repeat. The characteristics of Mesoform 1 are appropriate for mud drape deposits composed of laminated, sandy silt that is relatively uniform. Thus, this mesoform is composed of a single microform type. The characteristics of Mesoform 2 are appropriate for trough cross-sets composed of alternating fine sand and medium sand. This mesoform is composed of two microforms: avalanche beds and interbeds. The global domain represents a portion of the deposits typical of point bars formed in curved alluvial streams. A single occurrence of Mesoform 2 overlain by Mesoform 1 would typically be within the range of 0.5–5 m thick. The vertical thickness of such sequences is strongly controlled by the depth of the depositing stream and the lateral extent is strongly controlled by its width.

$K_{Gok}$  is the geometric mean of conductivity within each microform type. The indicator scales of all microform units are assumed. The global mean log conductivity, variance and integral scale are  $M_Y = -0.807$ ,  $\sigma_Y^2 = 0.859$  and  $\lambda_Y = 8.36$  m.

The global semivariogram and covariance are given by Eqs. (4), (6) and (12) and displayed in Fig. 2. We define  $K_{G21} = K_{G22}$  and  $\rho = K_{G21}/K_{G11}$  to test the sensitivity of semivariogram and covariance to the contrast of mean conductivity. The other parameters are as in Table 2. When  $\rho = 1$  or  $K_{G11} = K_{G21} = K_{G22}$ , the cross terms or the second term on the RHS of Eq. (8) are 0 and the global semivariogram or covariance is made of only the auto terms (the sum of the productions of the auto transition probabilities and the auto semivariograms or auto covariances). When  $\rho$  increases, the contrast of mean conductivity of the different units increases so that the cross terms of the global semivariogram or covariance increase, while the auto terms remain constant and the same as that in the case of  $\rho = 1$ . When  $\rho = 5$ , the cross terms contribute more than half over the auto terms ( $\rho = 1$ ) in defining the global semivariogram and covariance.

#### 5.1. Evolution of the macrodispersion coefficients

Here we assume that the mean hydraulic gradient  $g_1$  is 1.0 and the porosity,  $n$ , is 0.3. The time evolution of the macrodispersion coefficients was plotted by using Eqs. (21)–(24) with the parameters listed in Table 2. This is given in Fig. 3. Two-dimensional longitudinal macrodispersion, at the initial stage, is smaller than 3D macrodispersion. The opposite is true for transverse macrodispersion. At the large-time limit, the 2D and 3D models approach each other.

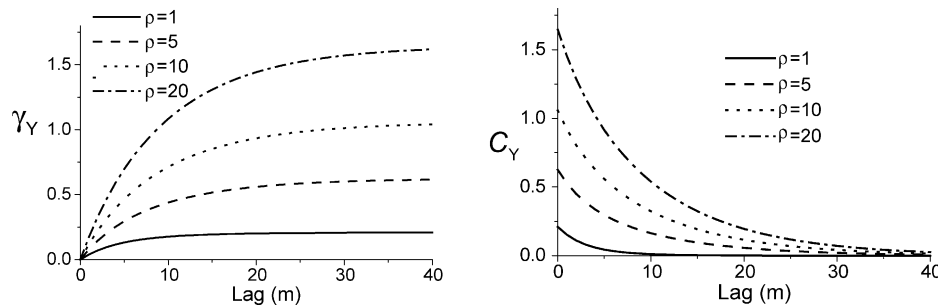


Fig. 2. The global semivariogram and covariance computed with Eqs. (4), (6) and (12). Here  $K_{G11} = 0.1$  m/d,  $K_{G21} = K_{G22}$  and  $\rho = K_{G21}/K_{G11}$ .

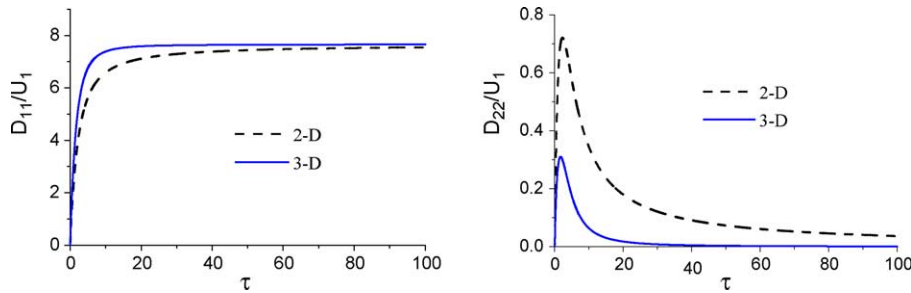


Fig. 3. The evolutions of the longitudinal and transverse macrodispersion coefficients in two- and three-dimensional domains ( $\varepsilon = 1$  and  $\tau = U_1 t / \lambda_l$ ).

Also,  $D_{22}/U_1$  approaches 0, which was also shown in a numerical simulation performed by Elfekei et al. (2002).  $D_{11}/U_1$  has the following, simplified expression

$$\frac{D_{11}(t)}{U_1} = \sum_{m=1}^3 \sum_{o=1}^N \sum_{k=1}^{N_o} \alpha_{mok} \eta_{mok}. \quad (25)$$

Eq. (25) and Table 1 show how different modes of contrast in log conductivity contribute on the macrodispersion at the large-time limit. They are not simply summed, but are weighted according to the proportions of different units.

### 5.2. Contributions of auto and cross terms

By using the parameters listed in Table 2, we computed the auto and cross terms of the macrodispersion coefficients from Eqs. (21)–(24). Fig. 4 shows that the auto ( $m = 1 + 2$ ) and cross ( $m = 3$ ) terms have the same shape as the longitudinal macrodispersion coefficients in 2D and 3D domains.

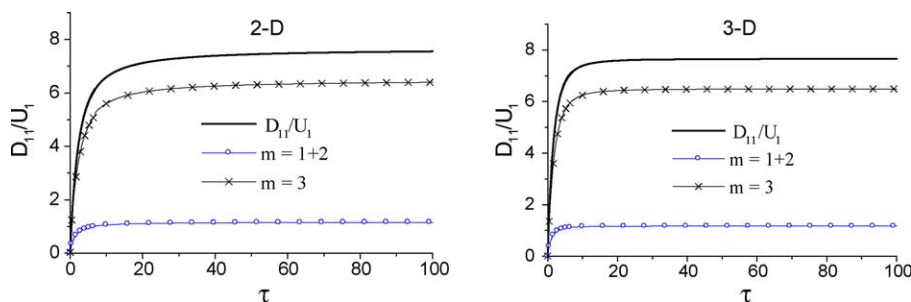


Fig. 4. The relative contributions of the auto and cross terms of  $D_{11}/U_1$  in two- (left) and three- (right) dimensional domains ( $\varepsilon = 1$  and  $\tau = U_1 t / \lambda_l$ ).

However, the cross terms have a much greater contribution to the macrodispersion coefficients than do the auto terms. Fig. 5 indicates that this is also true for the transverse macrodispersion coefficients. At the large-time limit, these coefficients are mainly made of cross terms and finally approach 0.

### 5.3. Sensitivity analysis

#### 5.3.1. Influence of the anisotropy ratio $\varepsilon$

The integration of Eqs. (18)–(20) was solved numerically using the parameters listed in Table 2. We fix  $\lambda_{ok}$  and  $\lambda_l$  as in Table 2 and allow  $\lambda_{zok}$  and  $\lambda_{zl}$  to vary with  $\varepsilon$ . The results with different  $\varepsilon$  are plotted in Fig. 6.

As Dagan (1989) observed for a unimodal domain, the anisotropy ratio  $\varepsilon$  here has a relatively small impact upon longitudinal macrodispersion in a hierarchical and multimodal domain, in which the units have a common anisotropy ratio. As  $\varepsilon$  increases, there is a slight decrease in  $D_{11}/U_1$  (Fig. 6A). On the other hand, the lateral and transverse macrodispersion

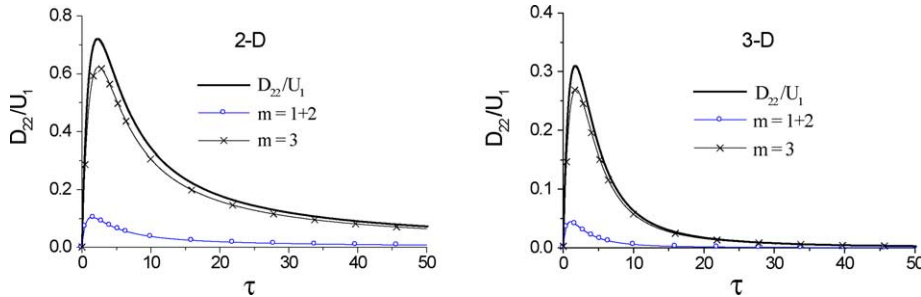


Fig. 5. The relative contributions of the auto and cross terms of  $D_{zz}/U_1$  in two- (left) and three- (right) dimensional domains ( $\varepsilon = 1$  and  $\tau = U_1 t/\lambda_I$ ).

coefficients increase significantly as the anisotropy ratio  $\varepsilon$  increases as shown in Fig. 6B and C.

5.3.2. Indicator scale  $\lambda_I$

In order to test the sensitivity of the macrodispersion coefficients to the indicator correlation scale  $\lambda_I$ , we let it vary from 1 to 20 and fix the other parameters at the values given in Table 2, and compute the macrodispersion coefficients according to Eqs. (21) and (22). The results are summarized in Fig. 7A and B.

Fig. 7A shows the macrodispersion coefficients are very sensitive to the indicator scale. When it

increases, the coefficients also increase. The evolution trends of the macrodispersion coefficients as  $\tau$  increases are very similar under different indicator scales. However, it is clear that the macrodispersion coefficients are scale-dependent parameters but not linear functions of the indicator scale.

When the macrodispersion coefficients are normalized by the flow velocity, global integral scale, and variance, these curves almost project to a single one (Fig. 7B). For  $D_{11}/U_1 \lambda_I \sigma_Y^2$ , the curves with different  $\lambda_I$  all approach unity, but the relative order of the curves is inverted from that of the corresponding

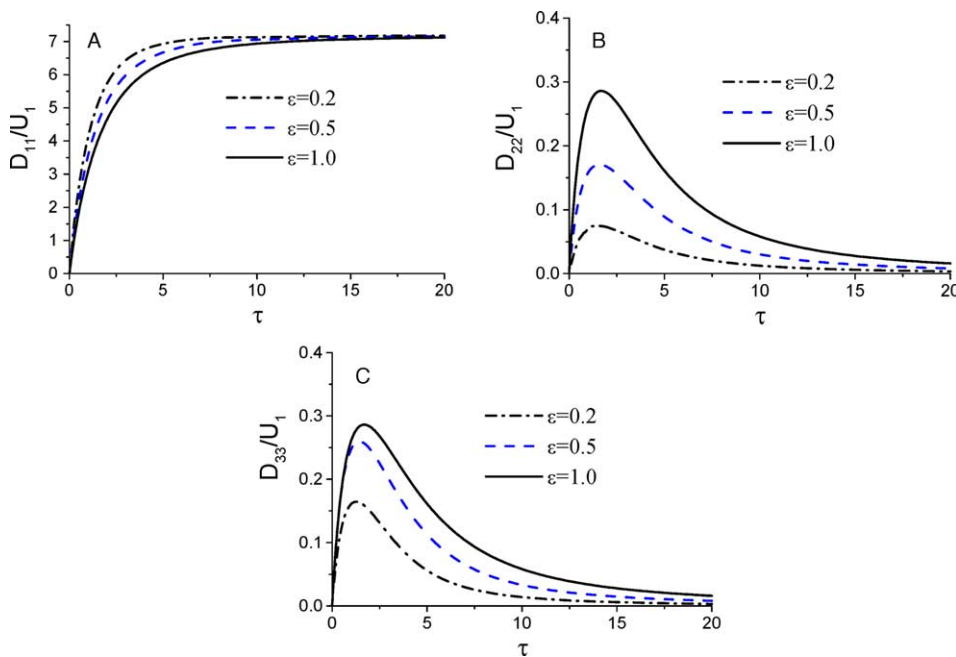


Fig. 6. The macrodispersion coefficients (A, longitudinal; B, lateral; C, transverse) as a function of the non-dimensional travel time  $\tau = U_1 t/\lambda_I$  with different  $\varepsilon$  values.

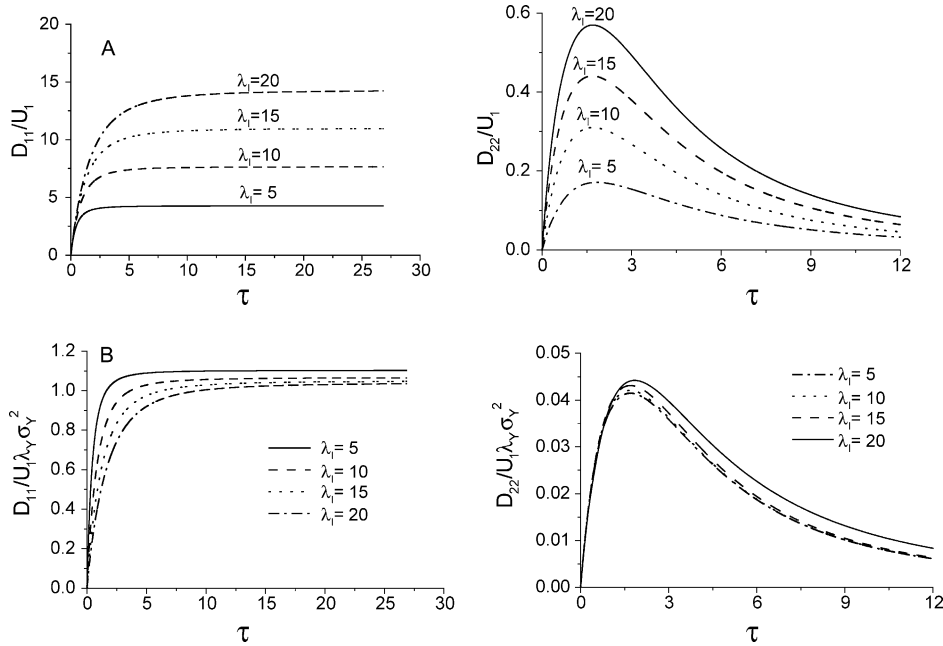


Fig. 7. (A) Sensitivity of the longitudinal and transverse macrodispersion coefficients to indicator correlation scale  $\lambda_I$  in three-dimensional domain ( $\varepsilon = 1$  and  $\tau = U_1 t / \lambda_I$ ). (B) Sensitivity of the normalized longitudinal and transverse macrodispersion coefficients to indicator correlation scale  $\lambda_I$  in three-dimensional domain ( $\varepsilon = 1$  and  $\tau = U_1 t / \lambda_I$ ).

curves in Fig. 7A. When the indicator scale,  $\lambda_I$ , increases, the normalized longitudinal macrodispersion  $D_{11}/U_1 \lambda_Y \sigma_Y^2$ , decreases because the global integral scale increases with the indicator scale faster than longitudinal macrodispersion. For  $D_{22}/U_1 \lambda_Y \sigma_Y^2$ , the curves have the same trend and order as their counterparts,  $D_{22}/U_1$ , but fall closer to each other.

### 5.3.3. Integral scales $\lambda_{ok}$

Values of the parameters  $\lambda_{ok}$  varying from 1 to 10 were used to test the sensitivity of the macrodispersion coefficients to these parameters. The other parameters are fixed at the values listed in Table 2. We compute the macrodispersion coefficients according to Eqs. (21) and (22). The results are summarized in Fig. 8A and B. Here  $\lambda_{11} = 1$  m,  $\lambda_{21} = \lambda_{22}$  and  $\omega = \lambda_{21}/\lambda_{11}$ .

Fig. 8A shows that when the contrast in the integral scales increases, the longitudinal and transverse macrodispersion coefficients also increase. Note that the indicator scale is directly multiplied with the cross terms, which dominate in

the macrodispersion coefficients, while the integral scales are multiplied with the auto terms. Therefore, the macrodispersion coefficients are less sensitive to the integral scales.

On the other hand, when the macrodispersion coefficients are normalized by the global variance and integral scale, the results collapse into a single curve (Fig. 8B). This curve represents the evolution trend of the dimensionless macrodispersion coefficients as  $\tau$  increases.

### 5.3.4. Mean conductivity $K_{Gok}$

The contrast in mean conductivity is one of the parameters to which the macrodispersion coefficients are most sensitive. Here  $K_{G11} = 0.1$  m/d,  $K_{G21} = K_{G22}$  and  $\rho = K_{G21}/K_{G11}$ . In Fig. 9A, when  $\rho = 1$  or  $K_{G11} = K_{G21} = K_{G22}$ , which is equal to  $m_{11} = m_{21} = m_{22}$ , the cross terms ( $m = 3$  in Table 1) are 0 and the macrodispersion coefficients are composed of only the auto terms ( $m = 1 + 2$  in Table 1). When  $\rho$  increases, the difference between mean conductivity of the different units increases and the values of cross terms

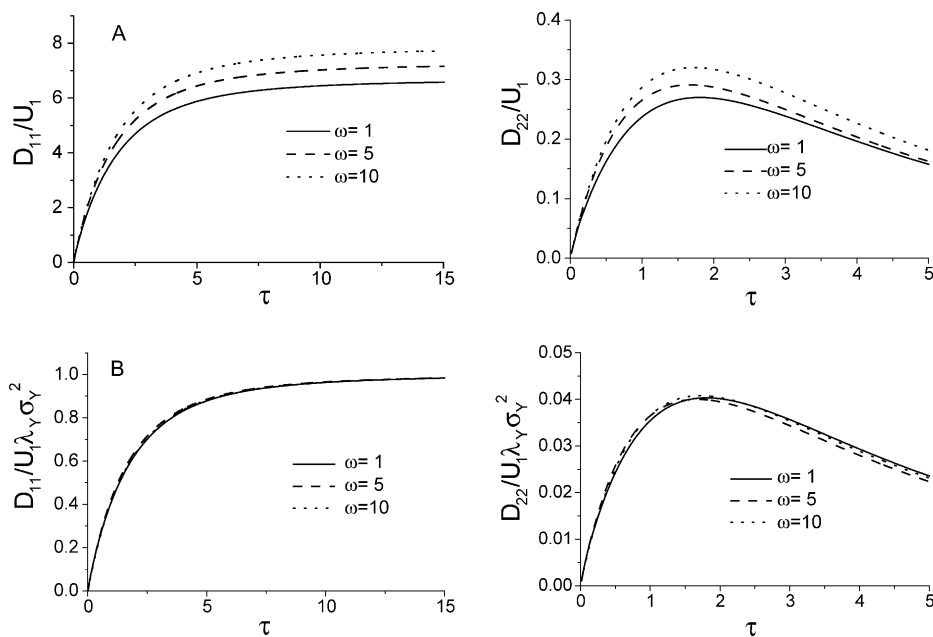


Fig. 8. (A) Sensitivity of the longitudinal and transverse macrodispersion coefficients to integral scales  $\lambda_{ok}$  in three-dimensional domain ( $\varepsilon = 1$  and  $\tau = U_1 t/\lambda_l$ ). (B) Sensitivity of the normalized longitudinal and transverse macrodispersion coefficients to integral scales  $\lambda_{ok}$  in three-dimensional domain ( $\varepsilon = 1$  and  $\tau = U_1 t/\lambda_l$ ).

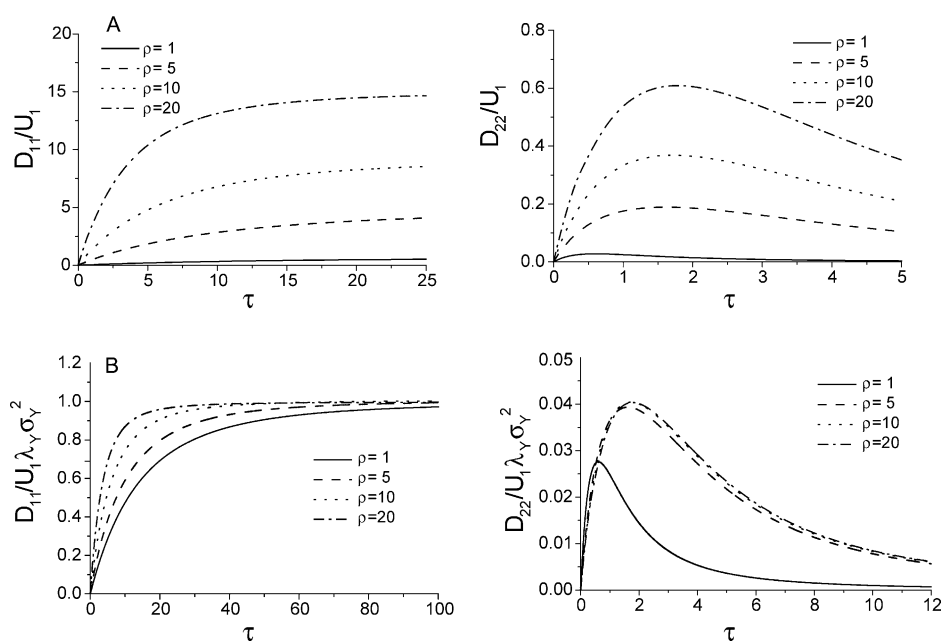


Fig. 9. (A) Sensitivity of the longitudinal and transverse macrodispersion coefficients to mean conductivity  $K_{Gok}$  in three-dimensional domain ( $\varepsilon = 1$  and  $\tau = U_1 t/\lambda_l$ ). (B) Sensitivity of the normalized longitudinal and transverse macrodispersion coefficients to mean conductivity  $K_{Gok}$  in three-dimensional domain ( $\varepsilon = 1$  and  $\tau = U_1 t/\lambda_l$ ).

of the macrodispersion coefficient increase. Therefore, both the non-normalized and normalized macrodispersion coefficients increase. In this case, the auto terms are constants and only the cross terms vary with  $\rho$ . The normalized transverse macrodispersion coefficient (Fig. 9B) with  $\rho = 1$  has a shape that differs from the others ( $\rho > 1$ ). It reaches its peak and reduces to zero much faster than the others. When  $\rho > 10$ , we can see that the cross terms start to dominate in the macrodispersion coefficients. In this situation, the contrast in conductivity between different units is high and the equations of macrodispersion coefficients can be simplified as those given below.

Note that when  $\rho > 10$ , the global variance is greater than unity (Fig. 2). This is outside of the small-variance assumption of the linear theory upon which our macrodispersion coefficients are derived. However, as stated by Glimm et al. (1993), Follin (1992) and Rubin (1997), the linear theory may give accurate estimates of mixing lengths for variance as large as 5, provided that the conductivity has a finite integral scale. In Fig. 9A and B, even when  $\rho = 20$ , the global variance ( $\sigma_y^2 = 1.65$ ) is much less than 5. Therefore, under these situations, our macrodispersion coefficients may give representative estimates for the solute transport.

In a hierarchical sedimentary system, there often is less variability of log conductivity within than between unit types because units represent similar depositional processes and environments that produce similar products (Koltermann and Gorelick, 1995). Desbarats (1990) presented a high contrast sand-shale sequence for flow and transport investigation, in which the variation of conductivity within the sandstone or shale was ignored.

Under the condition of high contrast in log conductivity ( $\rho > 10$ ), the second term in Eq. (8) is dominated and the first term may be ignored. Then, Eqs. (4) and (8) can be simplified as

$$\sigma_y^2 \approx \frac{1}{2} \sum_{o=1}^N \sum_{j=1}^N \sum_{k=1}^{N_o} \sum_{i=1}^{N_j} p_{ok} p_{ji} (m_{ok} - m_{ji})^2, \quad (26)$$

$$C_Y(\mathbf{h}) \approx \frac{1}{2} \sum_{o=1}^N \sum_{j=1}^N \sum_{k=1}^{N_o} \sum_{i=1}^{N_j} (m_{ok} - m_{ji})^2 \times p_{ok} (p_{ji} - t_{ok,ji}(\mathbf{h})). \quad (27)$$

The global covariance function can then be simplified as

$$C_Y(\tilde{h}) \approx \frac{1}{2} \sum_{o=1}^N \sum_{j=1}^N \sum_{k=1}^{N_o} \sum_{i=1}^{N_j} p_{ok} p_{ji} (m_{ok} - m_{ji})^2 e^{(-\tilde{h}/\lambda_I)} \\ = \sigma_y^2 e^{(-\tilde{h}/\lambda_I)}. \quad (28)$$

Eq. (28) indicates that the global covariance is linearly related to the global variance. Under this condition, the global integral scale is equal to the indicator correlation scale.

Furthermore, macrodispersion coefficients (21)–(24) in the isotropic case can be simplified for three dimensions as

$$\frac{D_{11}(t)}{U_1} = \sigma_y^2 \lambda_I \left\{ 1 + \frac{4}{e^\tau \tau^4} [6(e^\tau - \tau - 1) - \tau^2(e^\tau + 2)] \right\}, \quad (29)$$

$$\frac{D_{22}(t)}{U_1} = \frac{D_{33}(t)}{U_1} \\ = \sigma_y^2 \lambda_I \left\{ \frac{1}{e^\tau \tau^4} [12(1 + \tau - e^\tau) + \tau^2(5 + e^\tau + \tau)] \right\}, \quad (30)$$

and for two dimensions as

$$\frac{D_{11}(t)}{U_1} = \sigma_y^2 \lambda_I \left\{ 1 + \frac{3}{2e^\tau \tau^3} [2(e^\tau - \tau - 1) - e^\tau \tau^2] \right\}, \quad (31)$$

$$\frac{D_{22}(t)}{U_1} = \sigma_y^2 \lambda_I \left\{ \frac{6(1 - e^\tau + \tau) + 2\tau^2 + e^\tau \tau^2}{2e^\tau \tau^3} \right\}, \quad (32)$$

where  $\tau = tU_1/\lambda_I$  and  $\sigma_y^2$  is computed by Eq. (26). In this case, when time is sufficiently large,  $D_{22}/U_1$  in 2D and 3D domains still approaches 0, while  $D_{11}/U_1$  can be simplified as

$$\frac{D_{11}(t)}{U_1} = \sigma_y^2 \lambda_I \\ = \frac{\lambda_I}{2} \sum_{o=1}^N \sum_{j=1}^N \sum_{k=1}^{N_o} \sum_{i=1}^{N_j} p_{ok} p_{ji} (m_{ok} - m_{ji})^2. \quad (33)$$

Eq. (33) shows clearly a linear dependence of  $D_{11}$  on the global variance and indicator correlation

scale at the large-time limit. This result is the same as that of Gelhar (1993) except that Eq. (33) incorporates a hierarchical sedimentary structure. It should be noticed that Eqs. (29)–(33) are derived from the linear theory. Although, we noted previously that the small-variance assumption of the linear theory is robust for a variance as large as 5, a very large contrast in log conductivity would lead to a much larger variance. Kitanidis (1988) reported a complete breakdown of the linear theory at variance of the order of 20. So, these equations are only effective within the limited range of the global variance.

## 6. Conclusions

The major conclusions of this study are as follows:

1. The general global covariance functions in the isotropic and anisotropic cases have been developed by combining proportions, transition probabilities among categories, and covariances of log conductivity within sediments organized into three hierarchical levels. Exponential functions are assumed for the transition probabilities and the local covariances. Therefore, two types of correlation lengths are defined in the global covariance function: integral scale of log conductivity and indicator correlation scale.
2. The global integral scale is usually smaller than the indicator correlation scale. It is equal to the indicator correlation scale only when  $\sigma_{ok}^2 \rightarrow 0$ , or  $\lambda_{ok} = \lambda_l / \sqrt{p_{ok}}$  (for  $o = \overline{1, N}$ ;  $k = \overline{1, N_o}$ ), or when the contrast in the mean log conductivity between different units is relatively large.
3. The macrodispersion coefficients are derived for the solute transport in 2D and 3D domains. In the anisotropy 3D case, the ratio  $\varepsilon$  has a smaller impact upon the longitudinal macrodispersion coefficients than upon the lateral and transverse macrodispersion coefficients.
4. The values of macrodispersion coefficients vary with the changes of indicator correlation scale, integral scale, and the contrast of the mean log conductivity between different units. But, the macrodispersion coefficients are more sensitive to

indicator correlation scale than to the local integral scales.

5. The cross terms in the macrodispersion coefficients have an increasing contribution when the contrast of the mean conductivity between different units increases. Under the condition of high contrast in mean conductivity, only the cross terms contribute to the macrodispersion coefficients and the auto terms can be ignored. At the large time limit, the longitudinal coefficient shows clearly a linear dependence on the global variance and indicator correlation scale.

## Acknowledgements

This work was supported by the National Science Foundation under grants NSF-EAR 00-01125 and 00-01165. Any opinions, findings and conclusions or recommendations expressed in this paper are those of the authors and do not necessarily reflect those of the National Science Foundation. We thank Igor Jankovic and another anonymous reviewer for their constructive comments.

## Appendix A. The global covariance identity

When the cross-covariances in Eq. (7) are ignored, and

$$M_Y^2 = \left( \sum_{o=1}^N \sum_{k=1}^{N_o} p_{ok} m_{ok} \right)^2 = \sum_{o=1}^N \sum_{j=1}^N \sum_{k=1}^{N_o} \sum_{i=1}^{N_j} m_{ok} m_{ji} p_{ok} p_{ji}, \quad (A1)$$

then Eq. (7) can be rewritten as

$$C_Y(\mathbf{h}) = \sum_{o=1}^N \sum_{k=1}^{N_o} p_{ok} C_{ok,ok}(\mathbf{h}) t_{ok,ok}(\mathbf{h}) + \sum_{o=1}^N \sum_{j=1}^N \sum_{k=1}^{N_o} \sum_{i=1}^{N_j} m_{ok} m_{ji} p_{ok} (t_{ok,ji}(\mathbf{h}) - p_{ji}). \quad (A2)$$

The second term in the right hand side of Eq. (A2) can be replaced with

$$\begin{aligned}
 R &= \frac{1}{2} \sum_{o=1}^N \sum_{j=1}^N \sum_{k=1}^{N_o} \sum_{i=1}^{N_j} [(m_{ok} - m_{ji})^2 \\
 &\quad - m_{ok}^2 - m_{ji}^2] p_{ok} (p_{ji} - t_{ok,ji}(\mathbf{h})) \\
 &= \frac{1}{2} \sum_{o=1}^N \sum_{j=1}^N \sum_{k=1}^{N_o} \sum_{i=1}^{N_j} (m_{ok} - m_{ji})^2 p_{ok} (p_{ji} - t_{ok,ji}(\mathbf{h})) \\
 &\quad - \frac{1}{2} \sum_{o=1}^N \sum_{k=1}^{N_o} m_{ok}^2 p_{ok} \sum_{j=1}^N \sum_{i=1}^{N_j} (p_{ji} - t_{ok,ji}(\mathbf{h})) \\
 &\quad - \frac{1}{2} \sum_{j=1}^N \sum_{i=1}^{N_j} m_{ji}^2 \sum_{o=1}^N \sum_{k=1}^{N_o} (p_{ji} p_{ok} - p_{ok} t_{ok,ji}(\mathbf{h})) \quad (\text{A3})
 \end{aligned}$$

Because

$$\sum_{j=1}^N \sum_{i=1}^{N_j} (p_{ji} - t_{ok,ji}(\mathbf{h})) = 0 \quad \text{for } o = \overline{1, N}, k = \overline{1, N_o},$$

$$\sum_{o=1}^N \sum_{k=1}^{N_o} p_{ok} t_{ok,ji}(\mathbf{h}) = p_{ji} \quad \text{for } j = \overline{1, N}, i = \overline{1, N_j},$$

$$\sum_{o=1}^N \sum_{k=1}^{N_o} p_{ji} p_{ok} = p_{ji} \quad \text{for } j = \overline{1, N}, i = \overline{1, N_j},$$

Eq. (A3) can be simplified as

$$R = \frac{1}{2} \sum_{o=1}^N \sum_{j=1}^N \sum_{k=1}^{N_o} \sum_{i=1}^{N_j} (m_{ok} - m_{ji})^2 p_{ok} (p_{ji} - t_{ok,ji}(\mathbf{h})). \quad (\text{A4})$$

Finally, Eq. (A2) becomes

$$\begin{aligned}
 C_Y(\bar{h}) &= \sum_{o=1}^N \sum_{k=1}^{N_o} p_{ok} C_{ok,ok}(\mathbf{h}) t_{ok,ok}(\mathbf{h}) \\
 &\quad + \frac{1}{2} \sum_{o=1}^N \sum_{j=1}^N \sum_{k=1}^{N_o} \sum_{i=1}^{N_j} (m_{ok} - m_{ji})^2 \\
 &\quad \times p_{ok} (p_{ji} - t_{ok,ji}(\mathbf{h})). \quad (\text{A5})
 \end{aligned}$$

## Appendix B. Indicator correlation scale of transition probability

The transition probability is often expressed as an exponential function:

$$t_{ok,ji}(\mathbf{h}) = p_{ji} + (\delta_{ok,ji} - p_{ji}) e^{(-h_I / \lambda_{Iok,ji})} \quad (\text{B1})$$

for  $o, j = \overline{1, N}; k = \overline{1, N_o}; i = \overline{1, N_j}$ ,

$$\mathbf{h}_I = \sqrt{x^2 + y^2 + \varepsilon_I^{-2} z^2}, \quad \varepsilon_I = \lambda_{-I} / \lambda_{Iok,ji}.$$

Eq. (B1) must satisfy the following probability laws (Carle and Fogg, 1996):

$$\sum_{j=1}^N \sum_{i=1}^{N_j} t_{ok,ji}(\mathbf{h}) = 1, \quad \text{for } o = \overline{1, N}; k = \overline{1, N_o} \quad (\text{B2})$$

$$\sum_{o=1}^N \sum_{k=1}^{N_o} p_{ok} t_{ok,ji}(\mathbf{h}) = p_{ji} \quad (\text{B3})$$

for  $j = \overline{1, N}; i = \overline{1, N_j}$

Substituting the auto- and cross-transition probability in Eq. (B2) with the corresponding exponential functions in Eq. (B1), one can obtain

$$\begin{aligned}
 &\sum_{j=1}^N \sum_{i=1}^{N_j} t_{ok,ji}(\mathbf{h}) \\
 &= \sum_{j=1}^N \sum_{i=1}^{N_j} (p_{ji} + (\delta_{ok,ji} - p_{ji}) e^{(-h_I / \lambda_{Iok,ji})}) \\
 &= \sum_{j=1}^N \sum_{i=1}^{N_j} p_{ji} + \sum_{j=1}^N \sum_{i=1}^{N_j} (\delta_{ok,ji} - p_{ji}) e^{(-h_I / \lambda_{Iok,ji})} \\
 &= 1 + \sum_{j=1}^N \sum_{i=1}^{N_j} \delta_{ok,ji} e^{(-h_I / \lambda_{Iok,ji})} - \sum_{j=1}^N \sum_{i=1}^{N_j} p_{ji} e^{(-h_I / \lambda_{Iok,ji})} \\
 &= 1 + e^{(-h_I / \lambda_{Iok,ok})} - \sum_{j=1}^N \sum_{i=1}^{N_j} p_{ji} e^{(-h_I / \lambda_{Iok,ji})} \\
 &= 1 + \sum_{j=1}^N \sum_{i=1}^{N_j} p_{ji} (e^{(-h_I / \lambda_{Iok,ok})} - e^{(-h_I / \lambda_{Iok,ji})})
 \end{aligned}$$

for  $o = \overline{1, N}; k = \overline{1, N_o}$ .

Therefore,  $\sum_{j=1}^N \sum_{i=1}^{N_j} t_{ok,ji}(\mathbf{h}) = 1$ , if and only if  $\lambda_{Iok,ji} = \lambda_{Iok,ok}$  for  $o = \overline{1, N}; k = \overline{1, N_o}$ . This result

means that the auto- and cross-transition probabilities at the same row of the matrix have the same indicator correlation scale. Similarly, with Eq. (B3), we can obtain  $\lambda_{Ij_i,ok} = \lambda_{Ij_i,ji}$  for  $j = \overline{1, N}$ ;  $i = \overline{1, N_j}$ , or the auto- and cross-transition probabilities in the same column of the matrix have the same indicator scale. Finally, we obtain a uniform indicator correlation scale,  $\lambda_I$ , for all of the auto- and cross-transition probabilities in  $x, y$  plane

$$\lambda_{Iok,ji} = \lambda_{Ij_i,ok} = \lambda_I \quad (\text{B4})$$

for  $o, j = \overline{1, N}$ ;  $k = \overline{1, N_o}$ ;  $i = \overline{1, N_j}$ .

With the same process as above, we can prove in the vertical direction that the auto- and cross-transition probabilities also have a uniform indicator correlation scale  $\lambda_{zI}$ . According to Carle and Fogg (1996) and Ritzi (2000),  $\lambda_{zI} = \bar{l}_{ok}(1 - p_{ok})$ .  $\bar{l}_{ok}$  is the mean thickness of the sedimentary units of  $o$  mesor-form and  $k$  microform.

## References

- Barrash, W., Clemo, T., 2002. Hierarchical geostatistics, multi-facies systems, and stationarity: Boise Hydrogeophysical Research Site, Boise, Idaho. *Water Resour. Res.* 38(10), 1196doi: 10.1029/2002WR001436.
- Bridge, J.S., 2003. *Rivers and Floodplains: Forms, Processes, and Sedimentary Record*, Blackwell, Oxford, 491 pp.
- Carle, S.F., Fogg, G.E., 1996. Transition probability-based geostatistics. *Mathematical Geology* 28(4), 453–476.
- Carle, S.F., Fogg, G.E., 1997. Modeling spatial variability with one- and multi-dimensional continuous Markov chains. *Mathematical Geology* 29(7), 891–918.
- Cushman, J.H., Hu, X., Ginn, T.R., 1994. Nonequilibrium statistical mechanics of preasymptotic dispersion. *J. Stat. Phys.* 75, 859–878.
- Dagan, G., 1982. Stochastic modeling of groundwater flow by unconditional and conditional probabilities. 2. The solute transport. *Water Resour. Res.* 18(4), 835–848.
- Dagan, G., 1988. Time-dependent macrodispersion for solute transport in anisotropic heterogeneous aquifers. *Water Resour. Res.* 24, 1491–1500.
- Dagan, G., 1989. *Flow and Transport in Porous Formations*, Springer, New York, 465 pp.
- Dagan, G., 1994. Upscaling of dispersion coefficients in transport through heterogeneous formations, *Computational Method in Water Resources X*, Kluwer, Dordrecht, pp. 431–439.
- Dai, Z., Ritzi, R.W., Dominic, D.F., 2004. Estimating parameters in spatial correlation models for permeability in sediments with hierarchical organization. In: Hyndman, D.W., Bridge, J. (Eds.), *Aquifer Characterization*, SEPM Monograph, in press.
- Desbarats, A.J., 1990. Microdispersion in sand-shale sequences. *Water Resour. Res.* 26(5), 153–163.
- Di Federico, V., Neuman, S.P., 1998. Transport in multiscale log conductivity fields with truncated power variograms. *Water Resour. Res.* 34.
- Elfeki, A.M.M., Uffink, G.J.M., Barends, F.B.J., 1997. *Groundwater Contaminant Transport: Impact of Heterogeneous Characterisation, A New View on Dispersion*, A.A. Balkema, Rotterdam, 300 pp.
- Elfeki, A.M.M., Bruining, J., Kraaikamp, C., Dekking, F.M., 2002. Influence of fine-scale heterogeneity patterns on the large-scale behaviour of miscible transport in porous media. *Pet. Geosci.* 8, 159–165.
- Folin, S., 1992. Numerical calculations on heterogeneity of groundwater flow. PhD Dissertation. Royal Institute of Technology, Stockholm.
- Gelhar, L.W., 1993. *Stochastic Subsurface Hydrology*, Prentice-Hall, Englewood Cliffs, NJ.
- Glimm, J., Lindquist, W.B., Pereira, F., Zhang, Q., 1993. A theory of macrodispersion for the scale-up problem. *Trans. Porous Media* 13, 97–122.
- Kitanidis, P.K., 1988. Prediction by the method of moments of transport in a heterogeneous formation. *J. Hydrol.* 102, 453–473.
- Koltermann, C.E., Gorelick, S.M., 1995. Fractional packing model for hydraulic conductivity derived from sediment mixtures. *Water Resour. Res.* 31(12), 3283–3297.
- Leblanc, D.R., Garabedian, S.P., Hess, K.M., Gelhar, L.W., Quadri, R.D., Stollenwerk, K.G., Wood, W.W., 1991. Large scale natural gradient tracer test in sand and gravel. Cape Cod, Massachusetts. 1. Experimental design and observed tracer movement. *Water Resour. Res.* 27(5), 895–910.
- Lu, Z., Zhang, D., 2002. On stochastic modeling of flow in multimodal heterogeneous formations. *Water Resour. Res.* 38(10), 1190doi: 10.1029/2001WR001026.
- Neuman, S.P., 1990. Universal scaling of hydraulic conductivities and dispersivities in geologic media. *Water Resour. Res.* 26(8), 1749–1758.
- Neuman, S.P., 1997. Stochastic approach to subsurface flow and transport: a view to the future. In: Dagan, G., Neuman, S.P. (Eds.), *Subsurface Flow and Transport: A Stochastic Approach*, Cambridge Press, Cambridge, pp. 231–241.
- Ritzi, R.W., 2000. Behavior of indicator semivariograms and transition probabilities in relation to the variance in lengths of hydrofacies. *Water Resour. Res.* 36(11), 3375–3381.
- Ritzi, R.W., Dai, Z., Dominic, D.F., Rubin, Y., 2002. Spatial structure of permeability in relation to hierarchical sedimentary architecture in buried-valley aquifers: centimeter to kilometer scales. In: Findikakis, A., (Ed.), *Bridging the Gap Between Measurements and Modeling in Heterogeneous Media*, IAHS and Lawrence Berkeley Laboratory, (on CD-ROM).
- Ritzi, R.W., Dai, Z., Dominic, D.F., Rubin, Y., 2004. Spatial correlation of permeability in cross-stratified sediment with hierarchical architecture. *Water Resour. Res.*, 40, W03513, doi: 10.1029/2003WR002420.

- Rubin, Y., 1995. Flow and transport in bimodal heterogeneous formations. *Water Resour. Res.* 31(10), 1468–2461.
- Rubin, Y., 1997. Transport of inert solutes by groundwater: recent developments and current issues. In: Dagan, G., Neuman, S.P. (Eds.), *Subsurface Flow and Transport: A Stochastic Approach*, Cambridge Press, Cambridge, pp. 115–132.
- Rubin, Y., 2003. *Applied Stochastic Hydrogeology*, Oxford Press, Oxford.
- Rubin, Y., Journel, A.G., 1991. Simulation of non-Gaussian space random functions for modeling transport in groundwater, *Water Resour. Res.*, 27, 1711–1721.
- Rubin, Y., Sun, A., Maxwell, R., Bellin, A., 1999. The concept of block-effective macrodispersivity and a unified approach for grid-scale-and plume-scale-dependent transport. *J. Fluid Mech.* 395, 161–180.
- Russo, D., Zaidel, J., Laufer, A., 2001. Numerical analysis of flow and transport in variably saturated bimodal heterogeneous porous media. *Water Resour. Res.* 37, 2127–2141.
- Scheibe, T.D., Freyberg, D.L., 1995. The use of sedimentological information for geometric simulation of natural porous media structure. *Water Resour. Res.* 31, 3259–3270.
- Sudicky, E.A., 1986. A natural gradient experiment on solute transport in a sand aquifer: spatial variability of hydraulic conductivity and its role in the dispersion process. *Water Resour. Res.* 22(13), 2069–2082.
- Titzel, S., 1997. Quantification of the permeability distribution within sand and gravel lithofacies in a southern portion of the Miami Valley Aquifer. Masters Thesis. Wright State University.
- Zhang, D., 2002. *Stochastic Methods for Flow in Porous Media: Coping With Uncertainties*, Academic Press, San Diego, CA, 350 pp.
- Zhang, D., Lu, Z., 2001. Stochastic analysis of flow in a heterogeneous unsaturated-saturated system. *Water Resour. Res.* 38(2), 1018doi: 10.1029/2001WR000515.